Chemical Science

EDGE ARTICLE

View Article Online
View Journal | View Issue

Cite this: *Chem. Sci.*, 2019, **10**, 10740

All publication charges for this article have been paid for by the Royal Society of Chemistry

Received 17th July 2019
Accepted 4th October 2019

DOI: 10.1039/c9sc03521d

rsc.li/chemical-science

A lipidomic workflow capable of resolving *sn*- and C=C location isomers of phosphatidylcholines†

Xue Zhao,[a] Wenpeng Zhang,[b] Donghui Zhang,[c] Xinwei Liu,[c] Wenbo Cao,[c] Qinhua Chen,[d] Zheng Ouyang[c] and Yu Xia*[a]

As a major class of mammalian lipids, phosphatidylcholines (PCs) often contain mixtures of structural isomers, resulting from different lipogenesis pathways. Profiling PCs at the isomer level, however, remains challenging in lipidomic settings, especially for characterizing the positions of fatty acyls on the glycerol backbone (*sn*-positions) and the locations of carbon–carbon double bonds (C=Cs) in unsaturated acyl chains. In this work, we have developed a workflow for profiling PCs down to *sn*- and C=C locations at high coverage and sensitivity. This capability is enabled by radical-directed fragmentation, forming *sn*-1 specific fragment ions upon collision-induced dissociation (CID) of bicarbonate anion adducts of PCs ($[M + HCO_3]^-$) inside a mass spectrometer. This new tandem mass spectrometry (MS/MS) method can be simply incorporated into liquid chromatography by employing ammonium bicarbonate in the mobile phase without any instrument modification needed. It is also compatible with the online Paternò–Büchi reaction and subsequent MS/MS for the assignment of C=C locations in *sn*-1 fatty acyl chains of unsaturated PCs. The analytical performance of the workflow is manifested by identification of 82 distinct PC molecular species from the polar extract of bovine liver, including quantification of 19 pairs of *sn*-isomers. Finally, we demonstrate that five pairs of PC *sn*-isomers show significant compositional changes in tissue samples of human breast cancer relative to controls, suggesting a potential for monitoring PC *sn*-isomers for biomedical applications.

Introduction

Phosphatidylcholines (PCs) are a subclass of glycerophospholipids (GPs), accounting for more than 30% of the total lipid content in mammalian cells.[1] A majority of PCs function as structural components in the cell membrane, but many of them also actively participate in cell signaling[2] and gene regulation.[3] Cellular PCs are initially produced by *de novo* synthesis (Kennedy pathway), but later dynamically modified for fatty acyl compositions *via* a remodeling process (Lands' cycle).[4,5] The profile of PCs can serve as a readout of a certain biological state, which has found applications in tissue imaging[6] and marker discovery for human disease.[7,8] PCs are structurally diverse due to variations of fatty acyl chain lengths, *sn*-positions (relative positions of fatty acyls esterified on the glycerol backbone), or locations of carbon–carbon double bonds (C=Cs) in unsaturated fatty acyls. Thus, a single chemical formula of PC could contain a group of structural isomers. The number of reported PCs from a given lipidome, however, is typically less than 50, *e.g.*, 41 PCs from human plasma[9] and 14 PCs from yeast,[10] much less than that has been predicted.[11] One reason accounting for the small numbers of detected PCs arises from the fact that current lipid analysis methods do not differentiate structural isomers.

Mass spectrometry (MS) has become the tool of choice for lipid analysis by providing key information for lipid identification and quantitation at high sensitivity, coverage, and throughput.[8,12,13] Although high-resolution mass spectrometry allows determination of the molecular formula and thus lipid sum composition, detailed structural characterization still relies on obtaining characteristic fragment ions from tandem mass spectrometry (MS/MS).[14] Collision-induced dissociation (CID) is the most available and commonly used MS/MS technique for lipid identification, which can provide head group and fatty acyl composition information for GPs. Application of linked scans further enhances sensitivity and selectivity for lipid identification and quantitation from complex mixtures.[15] All the above conventional MS/MS methods have been routinely incorporated into various lipidomic analysis workflows, but they fall short for the analysis of lipid isomers down to *sn*- or C=C positions.

[a]*MOE Key Laboratory of Bioorganic Phosphorus Chemistry & Chemical Biological, Department of Chemistry, Tsinghua University, Beijing 100084, China. E-mail: xiayu@mail.tsinghua.edu.cn*

[b]*Department of Chemistry, Purdue University, West Lafayette, IN 47907, USA*

[c]*State Key Laboratory of Precision Measurement Technology and Instruments, Department of Precision Instrument, Tsinghua University, Beijing, 100084, China*

[d]*Affiliated Dongfeng Hospital, Hubei University of Medicine, Shiyan, Hubei Province 442000, China*

† Electronic supplementary information (ESI) available. See DOI: 10.1039/c9sc03521d

There has been a strong push from the MS community for developing methods capable of differentiating structural isomers, a step being considered critical to support the growth of lipidomics.[16,17] Localization of C=C has been recently achieved by paring C=C derivatization with subsequent MS/MS *via* CID, such as the Paternò–Büchì (PB) reaction[18,19] and epoxidation reaction.[20–22] These approaches are capable of determining C=C locations in various classes of lipids but they cannot provide information on the *sn*-positions of fatty acyls. Several MS/MS techniques utilizing ion activation/dissociation other than CID or combined with CID turn out to be quite informative for obtaining both *sn*-position and (or) C=C location from GPs. These include electron impact excitation of ions from organics (EIEIO),[23] ozone-induced dissociation (OzID),[24–26] and ultraviolet photodissociation (UVPD).[27,28] All these developments greatly expand the toolbox for lipid analysis; more importantly, they not only provide first-time analysis of lipidomes at the isomer level[11,19,28–30] but also demonstrate the link between altered isomer compositions with disease quantitatively and spatially.[31–34]

Radical-directed fragmentation has attracted increasing attention in MS/MS method development due to its unique capabilities in differentiating structural isomers of biomolecules, which otherwise cannot be obtained from charge-directed fragmentations typically seen from CID.[35,36] A common approach to induce radical-directed fragmentation from even-electron precursor ions, the most common ionic form derived from electrospray ionization (ESI), is to initiate homolytic cleavage of a covalent bond within the ion. Homolytic bond cleavage has been demonstrated for lipid analysis using photons,[35,37] electrons,[38] and radicals.[39] Reid and co-workers, however, showed that it was possible to induce radical-directed fragmentation from CID of anionic adducts of PC ions, such as methylcarbonate ($CH_3OCO_2^-$) and trifluoroacetate ($CF_3CO_2^-$).[40] We were thus motivated to explore radical-direct fragmentation *via* CID for PC analysis with a focus on evaluating its potential for differentiating *sn*-isomers. Although CID is not selective for inducing homolytic bond cleavages of unmodified bimolecular ions, we value its wide accessibility in commercial MS instruments. Such a method once developed would be MS platform independent and compatible with common existing lipidomic workflows.

In this work, we discovered that the bicarbonate anion (HCO_3^-) was bound strongly with the phosphocholine head group of PCs; thus, it facilitated homolytic bond cleavage (C–N bond) and formation of radical ions upon CID. These radical ions opened up an *sn*-specific fragmentation channel, forming diagnostic ions critical for identification and quantitation of *sn*-isomers. The MS/MS method allowed us to develop an LC-MS/MS workflow for high-throughput mapping of PCs within a lipidome at high sensitivity and coverage down to *sn*-positions and C=C locations, the latter of which was accomplished from incorporating PB-MS/MS. The workflow was evaluated by analyzing a polar lipid extract from bovine liver, with 82 distinct PC molecular species being identified, including 19 pairs of *sn*-isomers. It was further applied to profiling changes of PCs in cancerous human breast tissue. Five pairs of PC *sn*-isomers were found to exhibit significant changes, suggesting that PC lipogenesis was altered in human breast cancer tissue.

Results and discussion

MS/MS of bicarbonate adducts of PC anions *via* CID

In conventional lipid analysis workflows, PCs need to be analyzed in the form of anion adduct ions ($[M + A]^-$) in MS/MS to determine the composition of fatty acyl/alkyl, with acetate

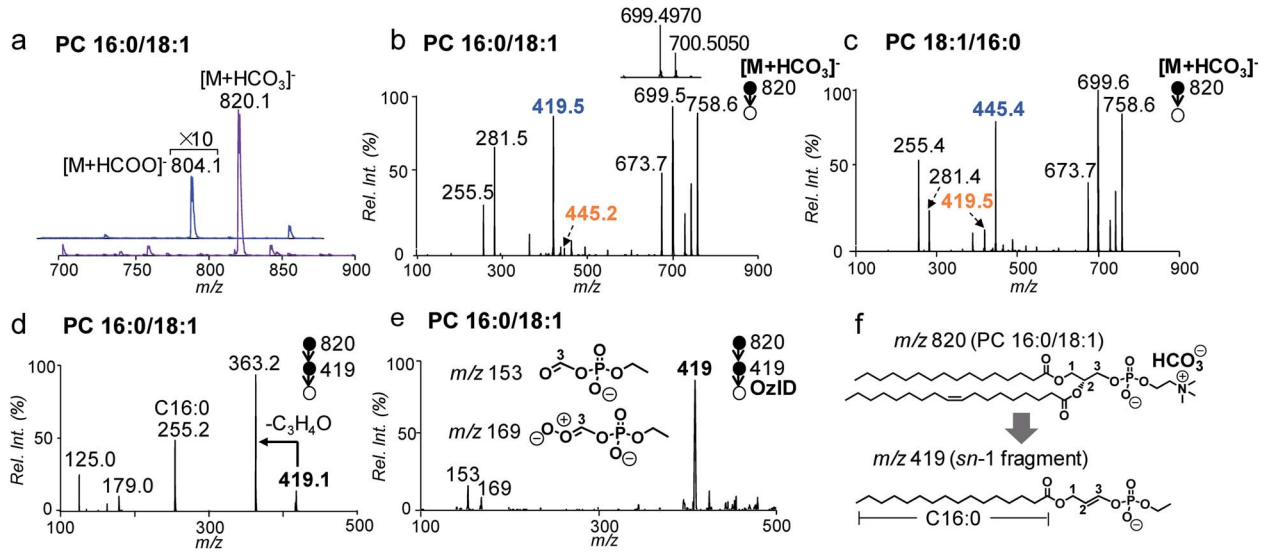

Fig. 1 (a) Negative ion mode nanoESI-MS^1 spectra of PC 16:0/18:1 (2 μM) from solutions containing 5 mM ammonium bicarbonate (NH_4HCO_3) and ammonium formate (NH_4COOH). (b) MS^2 CID of $[M + HCO_3]^-$ of PC 16:0/18:1 (*m/z* 820), CE = 30 eV. Inset: zoomed-in spectrum of fragments in *m/z* 699–701. (c) MS^2 CID of $[M + HCO_3]^-$ of PC 18:1/16:0 (*m/z* 820), CE = 30 eV. (d) MS^3 CID of fragment ions at *m/z* 419 from (b). (e) MS^3 OzID spectrum of *m/z* 419 from PC 16:0/18:1. (f) Proposed structure of the *sn*-1 fragment *m/z* 419 derived from CID of $[M + HCO_3]^-$ of PC 16:0/18:1.

(CH_3COO^-) and formate ($HCOO^-$) being the most commonly employed anions. MS^2 CID of PCs in negative ion mode can resolve *sn*-isomers due to a higher preference to lose *sn*-2 relative to the *sn*-1 chain as neutral ketene; however it suffers from low sensitivity due to weak binding between the quaternary ammonium headgroup and the anion.[41] In contrast, the bicarbonate anion (HCO_3^-) formed a strong adduct with the PC and thus led to more sensitive detection. Fig. 1a compares the nanoESI-MS spectra of PC 16:0/18:1 (2 μM) in negative ion mode derived from solutions containing 5 mM NH_4HCO_3 and NH_4-COOH, respectively. The $[M + A]^-$ ion signal from the bicarbonate adduct (*m*/*z* 820) is about 20 times higher than that of the formate adduct (*m*/*z* 804).

MS^2 CID of the bicarbonate adduct ions ($[M + HCO_3]^-$, *m*/*z* 820, Fig. 1b) produced several abundant fragments in the higher *m*/*z* region due to the loss of H_2CO_3 (−62 Da, *m*/*z* 758), combined losses of H_2CO_3 and $(CH_3)_3N$ (−121 Da, *m*/*z* 699), and loss of $HCO_3^{-\bullet}(CH_3)_3N^+ = CHCH_2$ (−147 Da, *m*/*z* 673). In the lower *m*/*z* region, fatty acyl anions, *i.e.* C16:0 (*m*/*z* 255) and C18:1 (*m*/*z* 281), were detected at lower relative abundances. The above fragmentation phenomenon is consistent with the main dissociation channels observed from CID of anion adducts of PCs reported by Reid and co-workers.[40] The main difference is that the fragment ions due to neutral loss of fatty acyl as ketene (NLK), signature from CID of formate anions of PCs, were not detected; instead, a new peak at *m*/*z* 419 was formed at relatively high abundance. The above set of data suggests that bicarbonate interacts with PCs differently as compared to formate and thus significantly alters the unimolecular dissociation chemistry of the PC anion adduct ions upon collisional activation (Fig. S1†).

We further examined MS^2 CID of the bicarbonate anion adduct of PC 18:1/16:0 (*m*/*z* 820, CE = 30 eV, Fig. 1c), the *sn*-isomer of PC 16:0/18:1. The two spectra were similar to each other, except that the peak at *m*/*z* 419 was much smaller, while the peak at *m*/*z* 445 was abundant. These differences indicate that fragment ions at *m*/*z* 419 or 445 might be correlated with the *sn*-positions of fatty acyls, which would be useful for structural determination. To characterize the identity of this new type of fragment ion, multi-stage tandem mass spectrometry, accurate mass measurements, and stable-isotope labeling were employed. Using the fragment peak at *m*/*z* 419 derived from PC 16:0/18:1 as an example, MS^3 CID of this peak produced *sn*-1 fatty acyl anions at *m*/*z* 255 (C16:0), suggesting that the *sn*-1 chain is preserved in the fragment (Fig. 1d and possible fragmentation pathways are shown in Scheme S1†). Based on the chemical formula derived from this ion ($C_{21}H_{40}O_6P$, Fig. S2†), a double bond or a ring structure should be generated. This fragment was subjected to OzID on a home-built linear ion trap mass spectrometer for structural elucidation (experimental details are provided in the ESI†). Two OzID fragments at *m*/*z* 153 and *m*/*z* 169 were observed (Fig. 1e), consistent with predicted ozonolysis products from a structure containing a double bond at C2–C3 of the glycerol backbone. Thus, a structure is proposed for the fragment ion *m*/*z* 419 (Fig. 1f), in which the *sn*-1 fatty acyl is connected to a dehydro-glycerol backbone while the C3-hydroxyl is esterified by ethyl phosphate. For simplicity of description, this type of ion is named as the *sn*-1 fragment, emphasizing that the *sn*-1 fatty acyl is preserved in such structures.

A comparison of the *sn*-1 fragment to the precursor ion (Fig. 1f) suggests that it cannot be generated by simple cleavages; instead, sequential fragmentation should be involved. We performed MS^3 CID of all major fragments within the *m*/*z* range 600–800 formed from MS^2 CID of the bicarbonate adduct of PC 16:0/18:1. The only one that produced *m*/*z* 419 as a major fragment in MS^3 CID was a radical ion at *m*/*z* 700.5 (data are provided in Fig. S3†). This species was formed at appreciable abundance right beside the fragment ion *m*/*z* 699.4970 when analyzed on a Q-TOF mass spectrometer (inset of Fig. 1b). Accurate mass measurement (*m*/*z* 700.5050) suggested an elemental composition of $C_{39}H_{73}O_8P^{-\bullet}$ (relative error: 1.8 ppm), likely resulting from combined losses of H_2CO_3 and the *N*,*N*-dimethyl aminomethyl radical ($(CH_3)_2N–CH_2^\bullet$) from the precursor ion ($[PC + HCO_3]^-$, $C_{43}H_{83}NO_{11}P$). This process should generate a carbon centered radical ion. Indeed, when this type of radical ion was allowed to react with residual oxygen in the ion trap for 200 ms, a peak corresponding to O_2 addition was clearly detected (data are provided in Fig. S4†). This ion/molecule reaction phenomenon is similar to those reported for carbon-centered peptide radical ions.[42]

A possible fragmentation pathway for forming the *sn*-1 fragment from CID of $[PC + HCO_3]^-$ anions is proposed in Scheme 1. Firstly, the bicarbonate anion in the ion complex abstracts a methyl proton in choline and leaves as H_2CO_3, which is supported by MS^2 CID of the bicarbonate adduct of d9-PC 16:0/16:0 (all nine choline hydrogen atoms are labeled with deuterium, Fig. S5†). The process is followed by homolytic cleavage of the C–N bond leading to a neutral loss of $(CH_3)_2N–CH_2^\bullet$. These two losses (120 Da) collectively lead to the formation of an ethyl radical on the remaining lipid anion ($C_{39}H_{73}O_8P^\bullet$ shown in Scheme 1). The ethyl radical then abstracts C3–H on the glycerol backbone; subsequent β-cleavage gives rise to neutral loss of *sn*-2 fatty acyl as $^\bullet R_2$ and CO_2

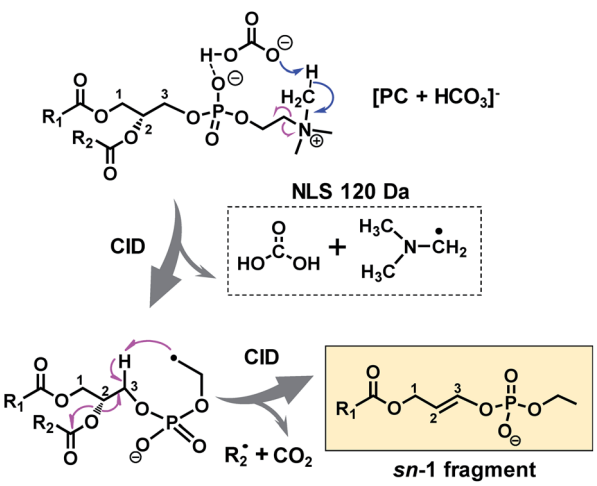

Scheme 1 Radical-directed fragmentation pathway for forming the "*sn*-1 fragment" from CID of bicarbonate adducts of PCs.

(ref. 43) and forms a double bond between C2 and C3 on the glycerol backbone. Given that this radical fragmentation channel is not observed from CID of formate or acetate adduct anions of PCs, we hypothesize that the –OH group in bicarbonate may form a relatively strong hydrogen bond with phosphate oxygen in PC molecules (possible interaction is indicated in Scheme 1). This hydrogen bonding may be critical to stabilize the ion complex and facilitate radical-directed fragmentation. Given the scope of this work, we did not persue molecular modeling to define the transition states involved in each fragmentation step; therefore, Scheme 1 should be viewed as a simplified pathway for the formation of the *sn*-1 fragment ion. An alternative fragmentation pathway involving the zwitterion intermediate is suggested in Scheme S2,† which might be favorable for lowering the barrier to homolysis of the C–N bond.

It is worth pointing out that the radical-directed fragmentation is *sn*-specific. Although ions at *m*/*z* 445 and *m*/*z* 419 were each detected at low abundances in CID of PC 16:0/18:1 (Fig. 1b) and PC 18:1/16:0 (Fig. 1c), they were later proved to be the "*sn*-1 fragments" resulting from corresponding *sn*-isomers, which are present as minor impurities in the supplied samples. We also note that this radical-directed fragmentation channel is promoted under higher energy CID conditions. For instance, no *sn*-1 fragments could be detected under on-resonance dipolar activation conditions (so-called ion trap CID) (Fig. S6†). This trend was observed for a series of PCs regardless of the chain lengths or the number of C=Cs in fatty acyls (Fig. S7†). This aspect further supports that strong H bonding between bicarbonate and the phosphate choline headgroup in the PC is key for the ions to access higher energy of activation under CID, which promotes the radical-directed fragmentation as compared to low-energy CID conditions.

Identification and quantitation of PC *sn*-isomers

The specificity of producing *sn*-1 fragments from CID of bicarbonate adducts of PCs provides a possibility of distinguishing and quantifying *sn*-isomers. Being aware of that the commercially obtained PC standards contain *sn*-isomers as minor impurities, we first measured the purity (% mol) of PC standards using the gold-standard, PLA_2 hydrolysis method. For all samples tested, the *sn*-purity% falls in the range of 80–95%, agreeing well with previous reports.[25,27] For instance, the *sn*-purity of the PC 16:0/18:1 sample is 93 ± 2%, meaning that it contains 7 ± 2% PC 18:1/16:0. This measurement also explains the detection of a low abundance peak at *m*/*z* 445 from the PC 16:0/18:1 sample (Fig. 1b), which is actually the *sn*-1 fragment derived from PC 18:1/16:0. The same discussion applies for a small peak at *m*/*z* 419 from the PC 18:1/16:0 sample (Fig. 1c), which contains 13 ± 2% *sn*-isomers. Using the purity information, we prepared a series of standard solutions containing different molar compositions of *sn*-isomers and subjected them to the analysis by MS^2 CID of $[M + HCO_3]^-$. Fig. 2a shows data acquired from the 2 : 1 mixture of PC 16:0/18:1 and PC 18:1/16:0 (total concentration kept at 10 μM). The relative ion abundance of the *sn*-1 fragment of PC 18:1/16:0 (*m*/*z* 445) was normalized to the sum of *sn*-1 fragments of both isomers and plotted against

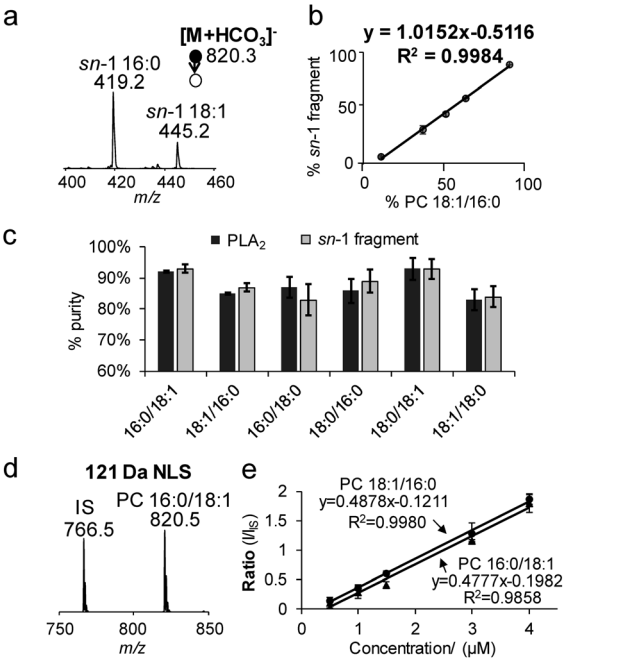

Fig. 2 (a) MS^2 CID spectrum of $[M + HCO_3]^-$ derived from a 2 : 1 mixture of PC 16:0/18:1 and PC 18:1/16:0. Only the *m*/*z* region of *sn*-1 fragment ions is shown. (b) Correlations between % *sn*-1 18:1 ions (I_{445}/(I_{445} + I_{419}) ×100) as a function of mol% of PC 16:0_18:1 with C_{total} kept at 10 μM. (c) Comparisons of the purity of six PC standards measured by the *sn*-1 fragment and PLA_2 method. (d) 121 Da NLS of a mixture containing 3 μM PC 16:0/18:1 and 2.5 μM IS, PC 15:0/15:0. (e) Quantitation for PC 16:0/18:1 and PC 18:1/16:0 from 121 Da NLS with IS (PC 15:0/15:0) kept at 0.5 μM.

corresponding concentrations (% mol) (Fig. 2b). An excellent linear relationship ($R^2 = 0.9984$) with a slope close to unity (1.02 ± 0.01) was achieved. Such a linear correlation was consistently observed for all six PC standards measured (Fig. S8†). Furthermore, the average % deviation of purities measured by the *sn*-1 fragment from that of the PLA_2 method was within ±2% for all six PC standards (Fig. 2c and Table S1†). These values compare favorably with *sn*-isomer quantitation reported by Ekroos *et al.* *via* MS^3 CID of $[M + HCO_2]^-$ of PCs, which shows a consistent negative deviation in the range of −1% to −7% (Table S2†).[41] The small system deviation associated with the *sn*-1 fragment ion method suggests that the relative ion abundance of the *sn*-1 fragment measured in a MS/MS spectrum can be directly used for quantitation of *sn*-isomers.

121 Da NLS for profiling and quantitation of PCs

Neutral loss of 121 Da (combined losses of H_2CO_3 and $N(CH_3)_3$) was a facile fragmentation channel from CID of PC bicarbonate adduct anions. It also showed high specificity to the choline head group as compared to other fragments, *i.e.* loss of 62 Da (H_2CO_3); therefore, it was tested for profiling of PCs from complex mixtures. The limit of detection (LOD) was estimated to be 10 pM from 121 Da NLS of the bicarbonate adduct of PC 16:0/18:1, based on a signal-to-noise ratio (S/N) greater than 3 (Fig. S9a†). Although this LOD was about 5 times higher than

that obtained from PIS *m/z* 184 (phosphocholine head group ion) of protonated PC 16:0/18:1 (Fig. S9b†), it was significantly more sensitive than the use of formate or acetate anion adduct ions (Fig. S9c†).

Neutral loss of 121 Da (Fig. 2d) also allowed achieving quantitation of PCs and their *sn*-isomers in a simple fashion. Fig. 2e compares calibration curves resulting from 121 Da NLS for PC 16:0/18:1 and PC 18:1/16:0 with PC 15:0/15:0 used as the internal standard (IS, 0.5 μM). Besides the excellent linearity of each plot, one most important feature is that the calibration curves of the two *sn*-isomers almost overlay with each other. These results suggest that the *sn*-positions of fatty acyls do not have a significant impact on the 121 Da NLS fragmentation channel for PCs. Moreover, hypothesis testing of the covariances and slopes of the two calibration curves suggest that they are not statistically different (testing details are provided in the ESI†). Thus, a calibration curve generated from 121 Da NLS of any *sn*-isomer can be used for quantitation of the sum concentration of a mixture of the two *sn*-isomers, greatly simplifying the overall procedure. Once the total quantity of the *sn*-isomers is found, quantitation of the isomers can be obtained by measuring their corresponding % *sn*-1 fragment as described earlier in Fig. 2b. We also noticed that the identity of the fatty acyl chains in PCs, *i.e.* length or degrees of unsaturation, had an impact on ion response in 121 Da NLS (spectrum of an equimolar mixture of PC 15:0/15:0, PC 16:0/18:0, and PC 18:0/20:4 is shown in Fig. S10†). Therefore, calibration curve based on 121 Da NLS should be established for each individual PC species.

Pinpointing C=C locations in *sn*-specific fatty acyl chains of PCs

The Paternò–Büchì reaction coupled with subsequent MS/MS (PB-MS/MS) allows for pinpointing C=C locations in fatty acyls of PCs; however, it cannot differentiate *sn*-positions.[18,19] Therefore, we tested pairing CID of bicarbonate adducts of PCs with PB-MS/MS for the determination of C=Cs in *sn*-1 fatty acyls of PCs. The presence of ammonium bicarbonate did not have an obvious impact on the conversion rates of the PB reactions nor did the PB reactions show any preference to *sn*-positions (Fig. S11†). The conversions typically ranged between 30% and 40% within 10 s, similar to that obtained without bicarbonate addition. Using PC 18:1/16:0 as a model compound (10 μM, 50/50, v/v, acetone/H_2O with 5 mM NH_4HCO_3), the solution was subjected to offline PB reaction and collected for nanoESI in negative ion mode (experimental details are provided in the ESI†). The PB product at *m/z* 878 ($[^{PB}M + HCO_3]^-$) can be clearly detected (Fig. 3a). MS^2 CID of the PB product (*m/z* 878) (Fig. 3b) produced the PB modified *sn*-1 fragment at *m/z* 503, which had a characteristic mass increase of 58 Da due to acetone addition to the intact *sn*-1 fragment (*m/z* 445). MS^3 CID of *m/z* 503 produced the PB modified C18:1 at *m/z* 339 (Fig. 3c). Further activation (MS^4 CID) of this ion produced C=C diagnostic ions at *m/z* 171 and 197, providing definitive evidence that C=C is located at Δ9 of the *sn*-1 chain (C18:1) (Fig. 3d).

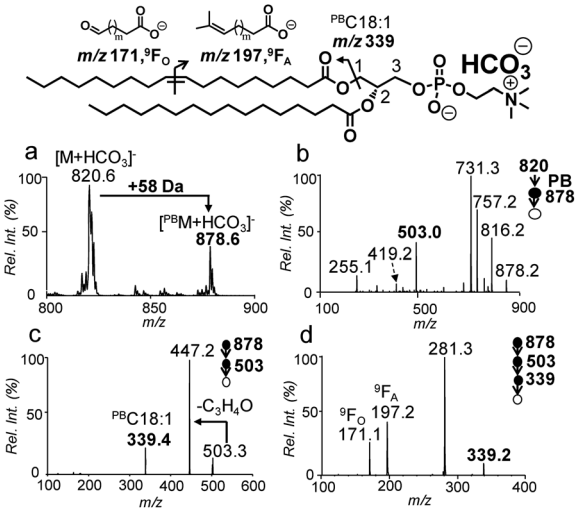

Fig. 3 (a) PB-MS of 10 μM PC 18:1/16:0 after 8 s UV irradiation. (b) PB-MS^2 *via* beam-type CID of ions at *m/z* 878. (c) PB-MS^3 ion trap CID of ions at *m/z* 503 from (b). (d) PB-MS^4 ion trap CID of $[^{PB}C\ 18:1]^-$ (*m/z* 339) from (c).

An LC-MS/MS workflow for the analysis of PCs down to *sn*- and C=C positions

The bicarbonate chemistry can be readily incorporated into an LC-MS/MS system. The platform consisted of HILIC-ESI-MS, in which an online photochemical reactor was installed post-column and right before ESI-MS.[30] The acetone/ACN/H_2O mobile phase system was used with NH_4HCO_3 added as buffer to assist the formation of anion adducts of PCs. Regarding lipid separation, use of NH_4HCO_3 as buffer in the mobile phase showed very similar performance to use of NH_4HCO_2 as buffer; however, detection of PCs in negative ion mode was significantly improved in the former case. Such a comparison can be found in Fig. S12,† using a polar lipid extract of bovine liver as an example. Data collection consisted of three LC-MS/MS runs (Fig. 4a). The first run employed 121 Da NLS in negative ion mode for PC subclass identification and relative quantitation. This run also provided a list of precursor *m/z* values of PCs ($[M + HCO_3]^-$), which was used to guide the second LC-MS/MS run in a targeted fashion. The second run (MS^2 CID of $[M + HCO_3]^-$) led to identification of PCs for fatty acyl composition, *sn*-position, and *sn*-isomer composition. Based on the above information, a list of precursor ions of unsaturated PCs was generated for the last run, LC-PB-MS^2 CID, for C=C location assignment. Note that we choose to perform LC-PB-MS^2 CID in positive ion mode because it is more sensitive on chromatographic timescale as compared to performing PB-MS^3 or MS^4 CID in negative ion mode. Consequently, the C=C location cannot be determined with *sn*-specificity. However, with known fatty acyl and *sn*-composition information, the C=C location can be assigned for PCs which do not contain major fatty acyl or *sn*-isomers. If the *sn*-1 unsaturated fatty acyl needs to be characterized, PB-MS^4 CID in negative ion mode needs to be performed in separate runs.

The analytical performance of the system was evaluated using a polar lipid extract from bovine liver (0.4 μg lipid

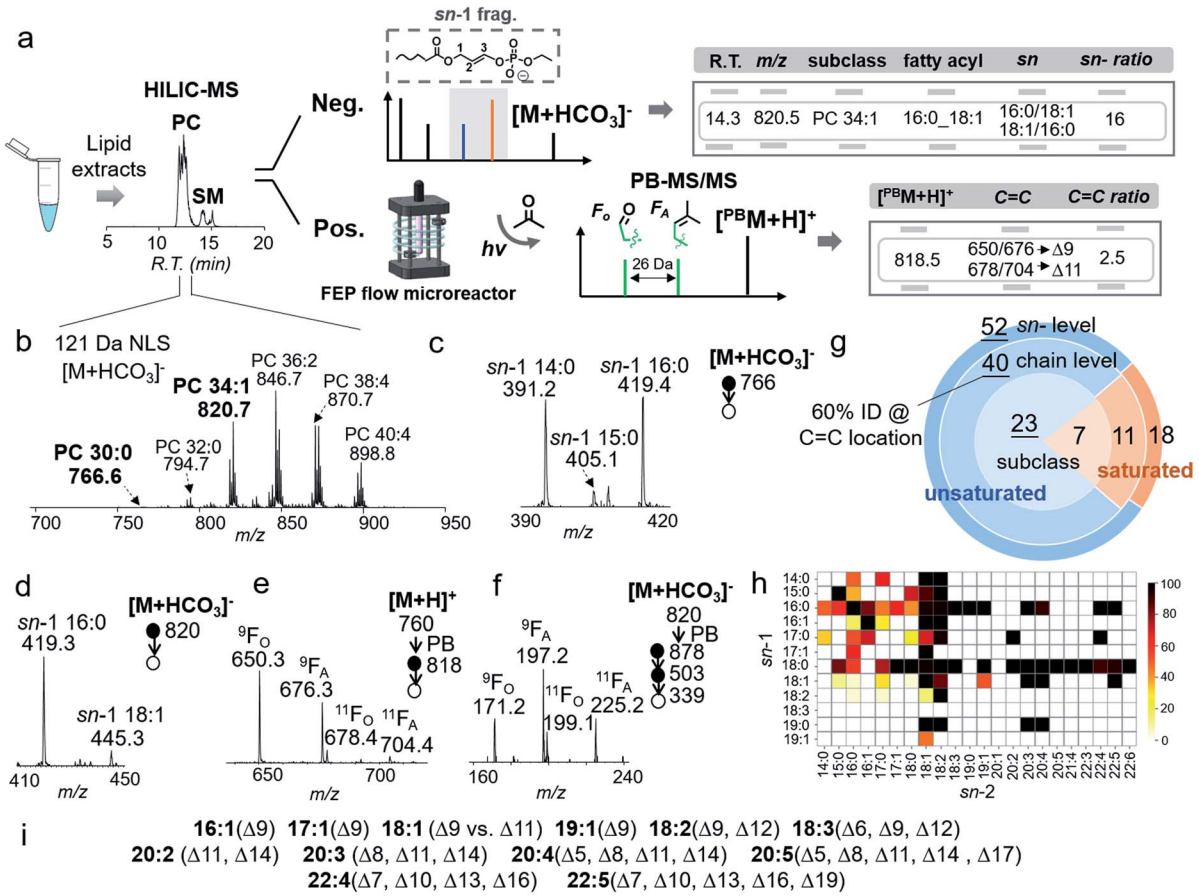

Fig. 4 (a) A HILIC-MS workflow for structural identification of PC in the bovine liver extract. (b) NLS 121 Da of $[M + HCO_3]^-$ of PCs from retention time 10.5–12.0 min in (a). MS^2 CID of $[M + HCO_3]^-$ of (c) PC 30:0 (*m/z* 766) and (d) PC 34:1 (*m/z* 820). (e) PB-MS^2 CID of PC 34:1 (*m/z* 818) in positive ion mode. (f) PB-MS^4 CID of $[^{PB}C\ 18{:}1]^-$ derived from PC 18:1/16:0. (g) The numbers of identified PCs from the bovine liver extract at different structural levels. (h) Heatmap of fatty acyls at *sn*-1 and *sn*-2 positions of identified PCs. (i) Identified C=C locations in unsaturated fatty acyls of PCs.

injection per run). HILIC provided separations of PCs from other classes of lipids (*i.e.*, PEs and SMs), while 121 Da NLS in negative ion mode provides the profile of PCs ($[M + HCO_3]^-$), leading to identification of 30 PCs at the subclass level (Fig. 4b). The coverage is the same as using PIS *m/z* 184 Da (Fig. S13†). Targeted MS/MS *via* beam-type CID identified PCs with the fatty acyl composition and *sn*-position. Taking PC 30:0 ($[PC + HCO_3]^-$, *m/z* 766) as an example, albeit at relatively low ion abundance (0.5%, normalized to PC 36:2, the most abundant PC in the bovine liver extract), HILIC-MS^2 CID produced high quality data for structural characterization. In the *m/z* region of *sn*-1 fragment ions (Fig. 4c), detection of ions at *m/z* 391 (*sn*-1 14:0), *m/z* 405 (*sn*-1 15:0), and *m/z* 419 (*sn*-1 16:0) proved that PC 30:0 contained three molecular species: PC 14:0/16:0, PC 16:0/14:0, and PC 15:0/15:0. The composition of the three species can be deduced as 47%, 47%, and 6%, respectively, according to the corresponding fractions of ion abundances.

HILIC-PB-MS/MS allowed determination of the C=C location in unsaturated PCs, which accounted for more than 80% of the identified PCs. Using PC 34:1 as an example, MS^2 CID of $[M + HCO_3]^-$ (*m/z* 820) suggested that it contained 94% PC 16:0/18:1 and 6% PC 18:1/16:0 (Fig. 4d). By applying the quantitation procedure described earlier, PC 16:0/18:1 was determined to be 1.7 ± 0.1 ng/(0.4 μg extract), while PC 18:1/16:0 was 0.1 ng/(0.4 μg extract). Given that PC 16:0/18:1 was the dominant component (94%), HILIC-PB-MS^2 CID in positive ion mode readily provided C=C location information, *viz.* Δ9 (major) and Δ11 (minor) for C18:1 at the *sn*-2 position (Fig. 4e). In order to pinpoint the C=C location of the minor *sn*-isomer (4%), PB-MS^4 CID was conducted. The zoomed-in region in Fig. 4f shows two pairs of C=C diagnostic ions (*m/z* 171, 197; *m/z* 199, 225) of C18:1, suggesting that PC 18:1/16:0 contains two C=C isomers, PC 18:1(Δ9)/16:0 and PC 18:1(Δ11)/16:0. Combining all the above information, it is evident that PC 16:0_18:1 contains four distinct molecular species, including two *sn*-isomers and two C=C location isomers of the C18:1. This level of detailed structural information would not be available from the conventional analysis workflow relying just on CID.

Using the workflow described above, 70 PCs were identified for *sn*-positions, including 19 pairs of *sn*-isomers (Fig. 4g). This is a significant increase as compared to 51 PCs identified at the fatty acyl level due to the improved capability of structural identification. Fig. 4h shows the heatmap of identified PCs

down to *sn*-positions; the color codes represent mol% of *sn*-isomers within the pair. It is evident that fatty acyls at the *sn*-1 position show lower diversity than those at the *sn*-2 position, with C16:0 and C18:0 as two high frequency groups. Although it has been suggested that the *sn*-2 position is preferred by polyunsaturated acyl chains,[29,44] our data quantitatively show that many of them still consist of minor *sn*-isomers, such as PC 20:4/16:0 (4%) and PC 22:4/18:0 (9%). For unsaturated PCs, about 60% were identified for C=C locations. The results for C=C determination in unsaturated fatty acyls are summarized in Fig. 4i. The most frequent C=C isomers are Δ9 and Δ11 isomers of C18:1 fatty acyl, while PUFAs are dominant by either ω-6 or ω-3 C=C locations, which are consistent with a previous report.[30] Counting identified C=C location isomers, a total of 82 PC molecular species were identified. The complete identification list is provided in ESI Data 1.†

Analysis of isomeric PCs from human breast cancerous tissue

Several recent MS imaging studies clearly demonstrated that lipid isomers, including fatty acyl compositional isomers, *sn*-, and C=C location isomers, were distributed heterogeneously in tissue sections or among different types of tissues, likely carrying distinct functions.[31–33,45] In an earlier study, we reported that changes of C=C location isomers were more sensitive to pathological conditions than lipid profile changes.[19] In this study, we were interested to test if changes of PC *sn*-isomers would differentiate lipidomes of diseased and healthy states, which may be potentially used as markers in biomedical and clinical studies.[46] Using the HILIC-LC-MS workflow described earlier, we thus evaluated this idea by analyzing PCs in cancerous human breast tissue samples ($N = 3$), while paracarcinoma tissue samples ($N = 3$) were used as controls (three technical repeats were acquired for each sample). Four levels of structural and quantitative analysis were performed for PCs, including subclass, fatty acyl composition, *sn*-composition, and C=C location. At the subclass level, 42 PC species were identified from NLS 121 Da of their bicarbonate adduct anions (Fig. S14a†). Among these, only PC 32:1 and PC 34:2 showed significant changes in relative ion abundances (IS: PC 15:0/15:0). This result was consistent with previous findings in which relative quantitation at the subclass level was obtained from PIS *m*/*z* 184.[30]

Application of HILIC-MS/MS led to identification of 80 PCs down to fatty acyl compositions and *sn*-positions (complete identification list is in ESI Data 2†). The identified PCs were found the same between normal and cancerous tissue, while their relative abundances and *sn*-isomer compositions varied. Among 26 pairs of PC *sn*-isomers, five showed significant changes in isomeric ratios ($P < 0.001$, average RSD = 22 ± 11%). These include PC 16:0_18:1, PC 16:0_16:1 (data are provided in Fig. S14b†), PC 15:0_18:1, PC 16:0_17:1, and PC 16:0_17:0. For instance, PC 16:0_17:0 was found to exhibit significant changes in *sn*-ratios ($P = 4.6 \times 10^{-7}$), accompanied by a large increase of PC 16:0/17:0 (65%) in cancerous tissue relative to control (15%) (Fig. 5d). Note that subclass profiling is blind to isomers and thus cannot differentiate fluctuations of each isomer when the summed abundances of the isomer pair are not significantly altered (Fig. 5a). Moreover, because PC 16:0_17:0 is a saturated lipid, it cannot be analyzed for C=C location isomers. A more challenging example is given by PC 33:1 (Fig. 5b). Beam-type CID revealed that it contained two fatty acyl compositional isomers: PC 16:0_17:1 (major) and PC 15:0_18:1 (minor). The compositional changes of the C18:1 Δ9 and Δ11 isomers of PC 15:0_18:1 were not statistically different between the normal and cancerous tissue samples.[30] In contrast, *sn*-position analysis revealed that both PC 16:0_17:1 and PC 15:0_18:1 contained *sn*-isomers and each pair of isomers showed significant changes between cancerous and normal breast tissues (Fig. 5b, e, and 5f). There were also cases that *sn*-isomers and C=C location isomers were both altered in cancerous tissue samples. PC 16:0_18:1 was one of the most abundant species in breast tissue and it was identified to consist of *sn*-isomers and C=C location isomers (Δ9 *vs.* Δ11 in C18:1). Relative to the control, the major *sn*-isomer PC 16:0/18:1 and the C=C location isomer C18:1(Δ9) were found to increase significantly in the cancerous tissue samples ($P = 3.5 \times 10^{-7}$ and $P = 2 \times 10^{-4}$, respectively, Fig. 5c, g and 5h). Notably, the same pair of *sn*-isomers was found to distribute distinctly in the tumor region relative to surrounding tissue in a mouse brain section, as recently revealed by OzID MALDI-imaging[31] and DESI-UVPD-

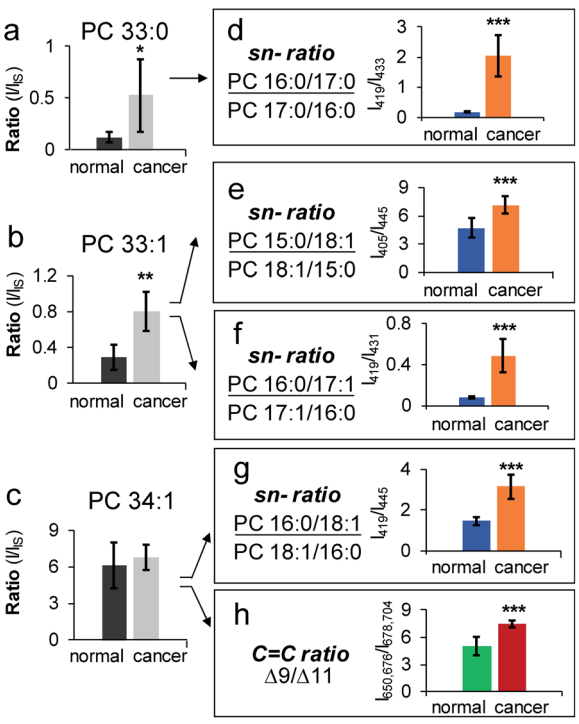

Fig. 5 Analysis of isomeric PCs in human breast tissue samples, cancerous *vs.* normal. Relative quantitation of (a) PC 33:0, (b) PC 33:1, and (c) PC 34:1 at the subclass level. Changes of *sn*-isomeric ratios of (d) PC 16:0_17:0, (e) PC 15:0_18:1, (f) PC 16:0_17:1, and (g) PC 16:0_18:1. (h) Relative ratio changes of C=C location isomers (Δ9/Δ11) of PC 16:0_18:1. Differences between the two groups of samples were evaluated for statistical significance using the two-tailed student's *t*-test (*$P < 0.05$, **$P < 0.01$, ***$P < 0.001$). Error bar represents ± s.d. ($N = 3$).

imaging.[33,45] Our data clearly suggest that PC 16:0_18:1 may contain four structural isomers from combinations of two *sn*-isomers and two C=C location isomers of the C18:1. Quantitative comparison of each individual isomer, however, is challenging for the current workflow because C=C isomeric ratios of the *sn*-2 fatty acyl chain cannot be measured independently. Pham *et al.* demonstrated monitoring of relative compositions of the same four isomers of PC 16:0_18:1 individually from MS/MS experiments containing different sequences of OzID and CID.[26] Another interesting aspect unveiled from *sn*-isomer measurements is that for the *sn*-isomers which demonstrate significant changes in cancerous tissue they all showed selective enrichment of *sn*-isomers containing unsaturated or odd carbon number fatty acyls at *sn*-2 positions. Although this trend needs to be verified with larger sampling size, it provides a new insight into the lipogenesis of PCs which is dynamically regulated by *de novo* synthesis and remodeling processes.[47,48] Collectively, the capability of monitoring changes of a large number of *sn*-isomers enables more sensitive detection of changes of PCs in diseased tissue samples, which is highly complementary to data obtained from subclass analysis (Fig. S14a†) or C=C location isomer analysis (Fig. S14c†).

Conclusions

In this study we have developed an LC-MS/MS workflow for identification and quantitation of PCs down to *sn*-positions with high lipid coverage and sensitivity (10 pM LOD). This unique capability is enabled by radical-directed fragmentation, forming *sn*-1 specific fragment ions upon CID of the bicarbonate anion adducts of PCs ($[M + HCO_3]^-$). It is worth noting that identities of fatty acyls, their *sn*-positions, and the quantity of *sn*-isomers can all be directly obtained from a single MS^2 CID spectrum. More importantly, PB-MS/MS can be merged into the LC-MS workflow, allowing determination of C=C locations in unsaturated fatty acyls of PCs. Using a polar lipid extract from bovine liver as a model system, 82 molecular species of PCs have been identified for *sn*-positions while a majority of unsaturated PCs have been identified for the locations of C=Cs. The capability of quantifying a variety of *sn*-isomers of PCs is an important addition for lipid biomarker discovery and it is highly complementary to monitoring compositional changes of C=C location isomers. Five pairs of PC *sn*-isomers were found to exhibit significant changes from human breast cancer tissue relative to the control. Interestingly, the changes of isomers showed a preference to sort unsaturated fatty acyls and odd numbers of carbons at the *sn*-2 position, which might be linked with altered PC biosynthetic pathways in human breast cancer. Regarding accessibility, the LC-MS/MS workflow should be highly compatible with existing LC and shotgun lipid analysis workflows, because it only requires an addition of ammonium bicarbonate to either the mobile phase or the lipid extract. Limited by the mechanism of forming *sn*-1 specific fragment ions, lipids which do not contain phosphocholine headgroups cannot be analyzed for *sn*-positions. Nevertheless, the success for PC analysis highlights the potential of using radical-directed fragmentation for lipid isomer analysis by mass spectrometry.

Conflicts of interest

There are no conflicts to declare.

Acknowledgements

Financial support from the National Natural Science Foundation of China (Grant No. 21722506 and No. 21621003) and NIH R01GM118484 is greatly appreciated.

References

1 K. Koichi, F. Michiya and N. Makoto, *BBA, Biochim. Biophys. Acta, Lipids Lipid Metab.*, 1974, **369**, 222–233.
2 A. Koeberle, H. Shindou, S. C. Koeberle, S. A. Laufer, T. Shimizu and O. Werz, *Proc. Natl. Acad. Sci. U. S. A.*, 2013, **110**, 2546–2551.
3 M. V. Chakravarthy, I. J. Lodhi, L. Yin, R. R. Malapaka, H. E. Xu, J. Turk and C. F. Semenkovich, *Cell*, 2009, **138**, 476–488.
4 H. Shindou and T. Shimizu, *J. Biol. Chem.*, 2009, **284**, 1–5.
5 H. Shindou, D. Hishikawa, T. Harayama, K. Yuki and T. Shimizu, *J. Lipid Res.*, 2009, **50**, S46–S51.
6 E. Marien, M. Meister, T. Muley, T. G. del Pulgar, R. Derua, J. M. Spraggins, R. Van de Plas, F. Vanderhoydonc, J. Machiels, M. M. Binda, J. Dehairs, J. Willette-Brown, Y. L. Hu, H. Dienemann, M. Thomas, P. A. Schnabel, R. M. Caprioli, J. C. Lacal, E. Waelkens and J. V. Swinnen, *Oncotarget*, 2016, **7**, 12582–12597.
7 M. Mapstone, A. K. Cheema, M. S. Fiandaca, X. G. Zhong, T. R. Mhyre, L. H. MacArthur, W. J. Hall, S. G. Fisher, D. R. Peterson, J. M. Haley, M. D. Nazar, S. A. Rich, D. J. Berlau, C. B. Peltz, M. T. Tan, C. H. Kawas and H. J. Federoff, *Nat. Med.*, 2014, **20**, 415–418.
8 K. Yang and X. Han, *Trends Biochem. Sci.*, 2016, **41**, 954–969.
9 P. Zacek, M. Bukowski, T. A. Rosenberger and M. Picklo, *J. Lipid Res.*, 2016, **57**, 2225–2234.
10 M. Bhuiyan, D. Tucker and K. Watson, *J. Microbiol. Methods*, 2014, **105**, 1–15.
11 D. L. Marshall, A. Criscuolo, R. S. E. Young, B. L. J. Poad, M. Zeller, G. E. Reid, T. W. Mitchell and S. J. Blanksby, *J. Am. Soc. Mass Spectrom.*, 2019, **30**, 1621–1630.
12 M. Wang, C. Wang, R. H. Han and X. Han, *Prog. Lipid Res.*, 2016, **61**, 83–108.
13 T. Hu and J. L. Zhang, *J. Sep. Sci.*, 2018, **41**, 351–372.
14 X. Han, K. Yang and R. W. Gross, *Mass Spectrom. Rev.*, 2012, **31**, 134–178.
15 K. Ekroos, I. V. Chernushevich, K. Simons and A. Shevchenko, *Anal. Chem.*, 2002, **74**, 941–949.
16 Y. H. Rustam and G. E. Reid, *Anal. Chem.*, 2018, **90**, 374–397.
17 T. Porta Siegel, K. Ekroos and S. R. Ellis, *Angew. Chem., Int. Ed.*, 2019, **58**, 6492–6501.
18 X. Ma and Y. Xia, *Angew. Chem., Int. Ed.*, 2014, **53**, 2592–2596.
19 X. Ma, L. Chong, R. Tian, R. Shi, T. Y. Hu, Z. Ouyang and Y. Xia, *Proc. Natl. Acad. Sci. U. S. A.*, 2016, **113**, 2573–2578.
20 Y. Feng, B. Chen, Q. Yu and L. Li, *Anal. Chem.*, 2019, **91**, 1791–1795.

21 Y. Zhao, H. Zhao, X. Zhao, J. Jia, Q. Ma, S. Zhang, X. Zhang, H. Chiba, S. P. Hui and X. Ma, *Anal. Chem.*, 2017, **89**, 10270–10278.
22 W. Cao, X. Ma, Z. Li, X. Zhou and Z. Ouyang, *Anal. Chem.*, 2018, **90**, 10286–10292.
23 J. L. Campbell and T. Baba, *Anal. Chem.*, 2015, **87**, 5837–5845.
24 M. C. Thomas, T. W. Mitchell, D. G. Harman, J. M. Deeley, J. R. Nealon and S. J. Blanksby, *Anal. Chem.*, 2008, **80**, 303–311.
25 R. L. Kozlowski, T. W. Mitchell and S. J. Blanksby, *Sci. Rep.*, 2015, **5**, 9243.
26 H. T. Pham, A. T. Maccarone, M. C. Thomas, J. L. Campbell, T. W. Mitchell and S. J. Blanksby, *Analyst*, 2014, **139**, 204–214.
27 P. E. Williams, D. R. Klein, S. M. Greer and J. S. Brodbelt, *J. Am. Chem. Soc.*, 2017, **139**, 15681–15690.
28 D. R. Klein and J. S. Brodbelt, *Anal. Chem.*, 2017, **89**, 1516–1522.
29 T. Baba, J. L. Campbell, J. C. L. Blanc, P. R. S. Baker and K. Ikeda, *J. Lipid Res.*, 2018, **59**, 910–919.
30 W. Zhang, D. Zhang, Q. Chen, J. Wu, Z. Ouyang and Y. Xia, *Nat. Commun.*, 2019, **10**, 79.
31 S. R. Ellis, M. R. L. Paine, G. B. Eijkel, J. K. Pauling, P. Husen, M. W. Jervelund, M. Hermansson, C. S. Ejsing and R. M. A. Heeren, *Nat. Methods*, 2018, **15**, 515–518.
32 A. Bednarik, S. Bolsker, J. Soltwisch and K. Dreisewerd, *Angew. Chem., Int. Ed.*, 2018, **57**, 12092–12096.
33 M. R. L. Paine, B. L. J. Poad, G. B. Eijkel, D. L. Marshall, S. J. Blanksby, R. M. A. Heeren and S. R. Ellis, *Angew. Chem., Int. Ed.*, 2018, **57**, 10530–10534.
34 M. Stahlman, H. T. Pham, M. Adiels, T. W. Mitchell, S. J. Blanksby, B. Fagerberg, K. Ekroos and J. Boren, *Diabetologia*, 2012, **55**, 1156–1166.
35 H. T. Pham and R. R. Julian, *Int. J. Mass Spectrom.*, 2014, **370**, 58–65.
36 F. Tureček and R. R. Julian, *Chem. Rev.*, 2013, **113**, 6691–6733.
37 H. T. Pham, T. Ly, A. J. Trevitt, T. W. Mitchell and S. J. Blanksby, *Anal. Chem.*, 2012, **84**, 7525–7532.
38 T. Baba, J. L. Campbell, J. C. Le Blanc, J. W. Hager and B. A. Thomson, *Anal. Chem.*, 2015, **87**, 785–792.
39 H. Takahashi, Y. Shimabukuro, D. Asakawa, S. Yamauchi, S. Sekiya, S. Iwamoto, M. Wada and K. Tanaka, *Anal. Chem.*, 2018, **90**, 7230–7238.
40 X. Zhang and G. E. Reid, *Int. J. Mass Spectrom.*, 2006, **252**, 242–255.
41 K. Ekroos, C. S. Ejsing, U. Bahr, M. Karas, K. Simons and A. Shevchenko, *J. Lipid Res.*, 2003, **44**, 2181–2192.
42 Y. Xia, P. A. Chrisman, S. J. Pitteri, D. E. Erickson and S. A. McLuckey, *J. Am. Chem. Soc.*, 2006, **128**, 11792–11798.
43 B. L. J. Poad, B. B. Kirk, P. I. Hettiarachchi, A. J. Trevitt, S. J. Blanksby and T. Clark, *Angew. Chem., Int. Ed.*, 2013, **52**, 9301–9304.
44 H. Martinez-Seara, T. Rog, M. Karttunen, I. Vattulainen and R. Reigada, *J. Phys. Chem. B*, 2009, **113**, 8347–8356.
45 D. R. Klein, C. L. Feider, K. Y. Garza, J. Q. Lin, L. S. Eberlin and J. S. Brodbelt, *Anal. Chem.*, 2018, **90**, 10100–10104.
46 M. Sans, J. Zhang, J. Q. Lin, C. L. Feider, N. Giese, M. T. Breen, K. Sebastian, J. Liu, A. K. Sood and L. S. Eberlin, *Clin. Chem.*, 2019, **65**, 674–683.
47 T. Harayama, M. Eto, H. Shindou, Y. Kita, E. Otsubo, D. Hishikawa, S. Ishii, K. Sakimura, M. Mishina and T. Shimizu, *Cell Metab.*, 2014, **20**, 295–305.
48 H. Kawana, K. Kano, H. Shindou, A. Inoue, T. Shimizu and J. Aoki, *BBA, Biochim. Biophys. Acta, Mol. Cell Biol. Lipids*, 2019, **1864**, 1053–1060.